Proc. 5th Int. Workshop New Photon-Detectors (PD18)
JPS Conf. Proc. **27**, 012004 (2019)
https://doi.org/10.7566/JPSCP.27.012004

MaPMT Relative Efficiency Measurements for the LHCb RICH Upgrade

Ayan BATYRKHANOV[1,2*] on behalf of LHCb RICH Collaboration[3]

[1]*Department of Chemistry and Biochemistry, University of Arizona, Tucson, AZ, USA*
[2]*Department of Physics, Nazarbayev University, Astana, Kazakhstan*
[3]*CERN, Geneva, Switzerland*

**E-mail: ayan.batyrkhanov@nu.edu.kz*

(Received March 25, 2019)

The Large Hadron Collider beauty experiment (LHCb) at CERN is aimed to study flavor-physics. The Ring Imaging Cherenkov detector system (RICH), which provides particle identification, have been operating successfully since 2010. During the second Long Shutdown of the LHC of 2019-2020, the RICH detectors will be upgraded to maintain the excellent PID performance with a five-fold increase of instantaneous luminosity. In addition, the detector will be readout at the full LHC bunch-crossing rate of 40 MHz using a flexible software based trigger. To cope with that changes the current hybrid photon detectors will be replaced by Hamamatsu R13472 multi-anode photomultipliers (MaPMT) with external brand new frontend electronics. The new photodetectors and the associated electronics have been subjected to calibration procedures. The high-voltage working point determination, relative efficiency measurements of MaPMT pixels and their calibration procedure for the RICH detector system will be presented.

KEYWORDS: LHCb RICH, MaPMT, detector upgrade, particle detectors, photon detectors

1. Introduction

The Ring Imaging Cherenkov detector system (RICH) upgrade [1] includes the replacement of hybrid photon detectors (HPDs) [2] by new Hamamatsu [3] R13472 multi-anode photomultipliers (MaPMTs). The scheme presented in Fig. 1 was used for MaPMT behavior studies. The setup comprises 16 MaPMTs combined into groups of four called elementary cells (EC), the frontend electronics including the CLARO ASICs [4] used to digitize the signal, and two digital boards. The readout is performed by using

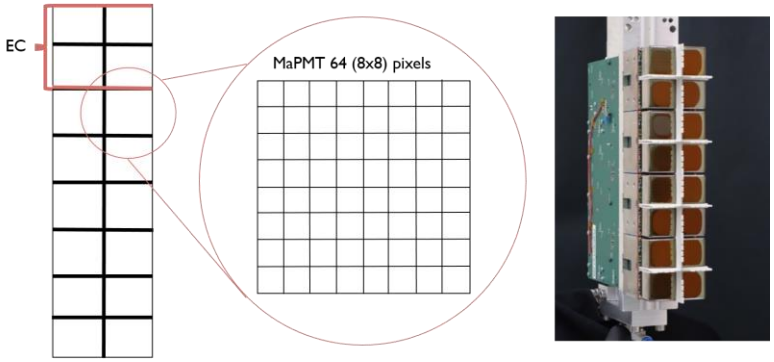

Fig. 1. MaPMT setup schematics (left) and the setup (right).

the prototype for the DAQ architecture of the upgraded LCHb experiment, namely the MiniDAQ2 [5] system. A stable illumination system is provided by a laser. This opto-electronics chain is the first level of modularity of the RICH upgrade detectors that can be integrated with the new LHCb readout architecture working at 40 MHz.

One MaPMT consists of 64 pixels, each pixel being coupled to a CLARO channel providing the digitization of the signal. The new photodetectors and the associated electronics have been subjected to calibration procedures that include the implementation of an algorithm to define the optimal working point for the RICH upgrade detectors. Operating voltages are investigated in order to optimize signal to noise ratio and ageing rate. This is achieved via determination of the average efficiency of the MaPMT channels as a function of High-Voltage (HV) applied to the MaPMT.

2. Determination of the Working Point for the Optoelectronics Chain and Relative Efficiency Measurement

2.1 Algorithm Development

The photon rate is measured for each programmable threshold of the readout chip to obtain the so-called S-curve (Fig. 2, right) that is the integral of the single-photon spectrum (Fig. 2, left). Single-photon spectrum varies from pixel to pixel due to the different gain, so MaPMT pixels have different S-Curve shape. Additionally, each associated CLARO channel has its own intrinsic offset. Therefore, pedestal positions and working points are different for each pixel of each MaPMT. The first step on efficiency measurements was to develop an algorithm to define the working point specifically for each pixel. Working point is the threshold at which the spectrum should be cut-off in order to avoid noisy signal and maximize the photon detection efficiency. This point lies in the valley region. CLARO allows visualizing the integrated spectrum through threshold scans. In order to zoom the necessary region offset was applied.

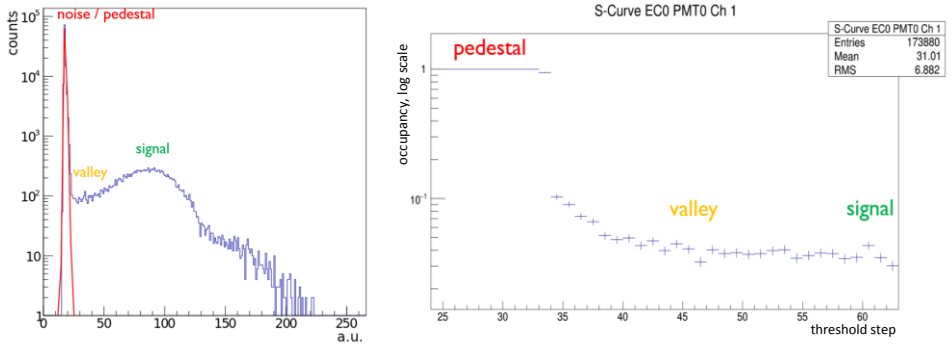

Fig. 2. Single photon spectrum (left) and normalized integral over spectrum at each threshold step that gives S-Curve (right).

To define the working value in order to have a high signal detection efficiency and a good spurious counts rejection the analyzed data is then fitted with linear plot to identify the sharp increase of the occupancy. This increase is associated with the closeness to pedestal and therefore gives nonlinear behavior. From the single photon spectrum on Fig. 2 it can be seen that the valley region is almost flat. S-Curve is a normalized integral under the curve of that spectrum at each threshold step. Therefore, at the valley region occupancy (the integral under the curve) does not change

significantly.

Linear plots were done on smoothed data starting with the fixed right end and moving the left end of the linear plot by one threshold step. The chi^2 test was chosen as an indicator of the nonlinearity of the plot. It can be easily seen that the value of chi^2 is increasing closer to the pedestal. Analyzing its evolution with respect to the threshold step, it is obvious that the slope of the chi^2 plot increases dramatically at some point (Fig. 3). The working point was chosen by cutting the data at the threshold step with chi^2 more than 4. To stay in the safe region working point was chosen as one threshold step closer to the signal than that cutting point.

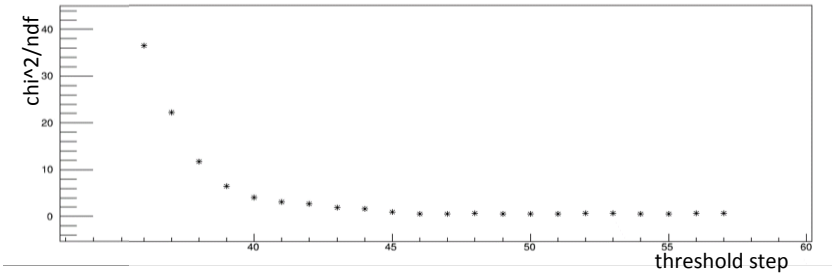

Fig. 3. Chi^2/ndf at various threshold steps plot to identify the working point.

2.2 Algorithm Validation

Necessity of the algorithm is proven by the fact that the working point is changing from pixel to pixel as well as the pedestal position. The algorithm was validated using the pedestal identification along with the width between the pedestal and the working value. Distributions of the pedestals and the width of the range were used as the validation at the different voltage values. Range should be consistent for all pixels and therefore their distribution should be narrow. Fig. 4 demonstrates narrow distributions that proves the validity of the working point identification algorithm.

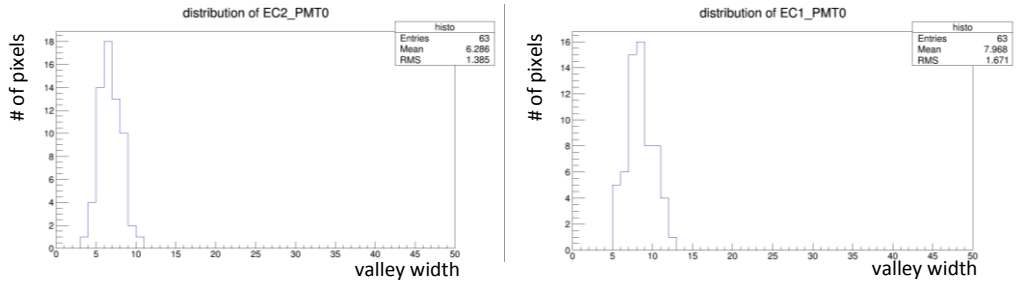

Fig. 4. Distribution of differences between working point found by algorithm and pedestals for different MaPMTs during one run.

3. Occupancy-HV Dependence

Using the distribution of differences between pedestals and working points (valley width) the evolution of valley width with voltage applied was studied. Valley width decreases with the voltage and that makes algorithm ineffective at the voltages less than 900V. Therefore, working point as 5 threshold steps from the pedestal was chosen for

850V and 800V runs. Occupancy at the working point is considered as an effective occupancy of the MaPMT pixel.

Results of the runs at the same voltage but at different times was averaged in order to include the laser instability effects. Occupancy of each MaPMT was taken as an average of all 64 pixels for that MaPMT. Occupancies for different voltages were normalized with respect to the value at 1000V and the plot can be seen in the Fig. 5 below. It shows almost linear response of the PMT's occupancy to the applied voltage. Large error bars occurs due to averaging 3 runs at each HV at different times during the day. Sharp difference between 850V and 900V is due to the different method of working point definition and therefore the average occupation calculation.

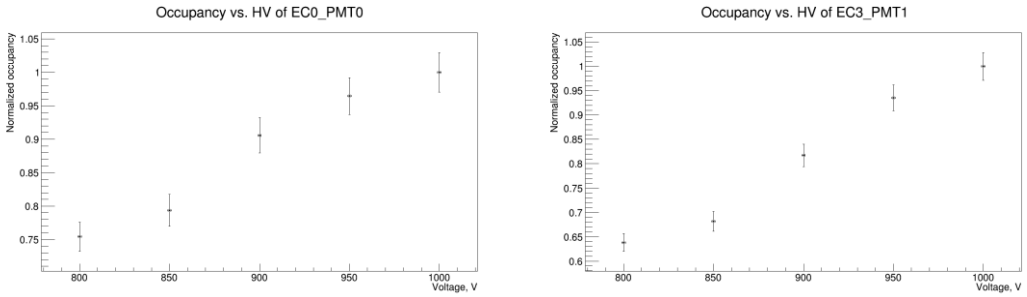

Fig. 5. Occupancy vs. HV plots for two different MaPMTs EC0 PMT0 (left) and EC3 PMT1 (right) averaged with respect to the average occupancy at 1000V.

4. Conclusion

Algorithm for the working point calculation was developed. The necessity for the working point calculation for each MaPMT pixel was validated by valley width and pedestal distributions. Relative efficiency dependence on the high-voltage applied at each MaPMT was recorded. Optimal voltage value for the experimental purposes can be identified using the obtained results. Future plans may require optimizing the algorithm for the working point calculation at low voltages.

References

[1] LHCb PID TDR LHCb collaboration, LHCb PID Upgrade Technical Design Report, CERN-LHCC2013-022. LHCb-TDR-014.
[2] T. Gys, et al. Nucl. Inst. Meth. A, 567 (2006), p. 176.
[3] Hamamatsu Photonics, 314-5 Shimokanzo, Toyookavillage, Iwatagun, Shizuokaken, 438-0193 Japan.
[4] P. Carniti, et al. JINST, 7 (2012), p. P11026.
[5] J-P Cachemiche et al., "Study for the LHCb upgrade readout board", JINST 5 (2010) C12036.